A Multi-MMC Coordinated Power Buffer Control Method for RES and Traction Load Fluctuations in FTPSS

1st Ruofan Li
School of Electrical engineering
Beijing Jiaotong University
Beijing, China
23111461@bjtu.edu.cn

2nd Mingchao Xia
School of Electrical engineering
Shenyang University of Technology;
Beijing Jiaotong University
Shenyang, China; Beijing, China
mchxia@bjtu.edu.cn
*Corresponding author

3rd Qianhao Sun
School of Electrical engineering
Beijing Jiaotong University
Beijing, China
sunqianhao@bjtu.edu.cn

4th Qifang Chen
School of Electrical engineering
Beijing Jiaotong University
Beijing, China
chenqf@bjtu.edu.cn

5th Yubin Wang
School of Electrical engineering
Beijing Jiaotong University
Beijing, China
ybwang@bjtu.edu.cn

6th Jichen Wang
School of Electrical engineering
Beijing Jiaotong University
Beijing, China
23111462@bjtu.edu.cn

***Abstract*—Power fluctuations from renewable energy sources and electric locomotives cause continuous operating-point disturbances in traction substation (TS) converters and energy storage systems in flexible traction power supply system (FTPSS). To mitigate this issue, this paper proposes a TS-level power buffering control method based on the coordinated operation of multiple modular multilevel converters (MMCs). Within an energy-coordinated control framework tailored for different converter types in the TS, the proposed method enables stable operation by responding only to the low-frequency components of external power disturbances. Moreover, an auxiliary energy-balancing control module introduces damping effects to ensure that the TS energy converges to its reference value. The effectiveness of the proposed control strategy is verified on a four-converter system modeled in MATLAB/Simulink, demonstrating its capability to suppress both small- and large-amplitude external power fluctuations.**

***Index Terms*—Flexible traction power supply system, power buffer, modular multilevel converter, power fluctuation, renewable energy sources, traction loads.**

I. Introduction

With the continuous advancement of railway electrification, renewable energy sources (RESs) and energy storage systems (ESSs) have been widely integrated into traction power supply systems (TPSSs) [1]. However, conventional TPSSs suffer from neutral zones, which reduce train operation efficiency and hinder the interconnection of RESs across feeding sections [2]. To address these issues, flexible traction power supply systems (FTPSSs) based on power electronic converters have become a major research focus in recent years, as illustrated in Fig. 1. In an FTPSS, RESs, ESSs, and trains (TRs) are comprehensively integrated within the traction substation (TS) [3]. Recent studies have investigated the optimal operation and control of FTPSSs incorporating RESs and ESSs. By flexibly allocating the power setpoints of supercapacitors and lithium-ion batteries, FTPSSs can maximize the absorption of RES power and regenerative braking energy, thereby reducing power purchase from the grid and improving system economy [4], [5]. Nevertheless, traction loads and renewable generation exhibit significant uncertainties and rapid power fluctuations, with traction loads capable of increasing by several megawatts within a few hundred milliseconds [6]. As a result, ESSs must rapidly adjust their operating points, which may violate the ramp-rate constraints of energy-type ESSs and increase the need for power-type ESSs.

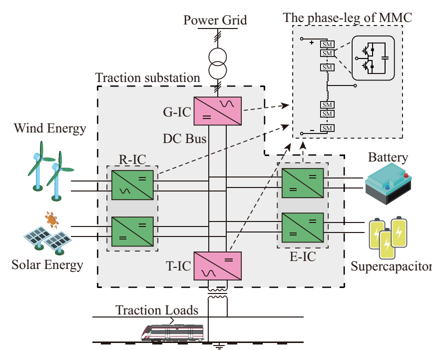

Fig. 1. MMC-Based FTPSS Traction Substation with Integrated RES and ESS.

This work was supported by the Key Program of the National Natural Science Foundation of China (Grant No. 52337003) and the Young Scientists Fund of the National Natural Science Foundation of China (Grant No. 52307210).

979-8-3315-8138-1

Given the strong competitiveness of the modular multilevel converter (MMC) in high-power energy conversion applications, all interlink converters (ICs) in FTPSS—including the RES interlink converter (R-IC), ESS (E-IC), traction (T-IC), and grid-side (G-IC)—can be implemented using MMC technology [7]. A promising approach to mitigating power disturbances caused by traction load variations and RES fluctuations is to exploit the electrostatic energy stored in the submodule capacitors of MMCs [8]. In the fields of high-voltage direct current transmission [9] and offshore wind power systems [10], existing studies have explored the energy utilization capability of MMCs. For instance, [11] demonstrated the independent controllability of MMC energy and DC voltage, while [10] and [12] developed inertia support and frequency regulation methods to suppress grid frequency deviations. However, these strategies generally superimpose an auxiliary MMC energy-response power component on the fundamental transmission power and deliver it to the AC grid, which is insufficient to meet the fluctuating power buffering demands of FTPSSs. Therefore, this paper proposes a TS-level power buffering control method based on multi-MMC coordinated energy control to suppress power fluctuations from both traction loads and renewable sources within the FTPSS.

II. Multi-MMC Coordinated Energy Control within the TS

As shown in Fig. 1, a TS within the FTPSS can be abstracted as being composed of four converters: G-, T-, E-, and R-IC. The G-IC acts as a slack bus that provides DC voltage to the DC bus and supports the AC sides of the remaining MMCs to operate in the grid-forming mode, thereby maintaining the external network voltage. Evidently, under the connection of traction loads and renewable energy sources (RESs), the AC-side power of the converters is determined by the external network and is subject to stochastic power disturbances. To address this issue, an MMC energy-utilization-based buffering control method for T/E/R-ICs, referred to as Vf-P, is proposed, as illustrated in Fig. 2(a). According to the DC- and AC-side powers of the converter, P_{dc} and P_{ac}, the total electrostatic energy stored in the MMC arms can be expressed as:

$$W_{\mathrm{t}} = \int (P_{\mathrm{dc}} - P_{\mathrm{ac}})\,\mathrm{d}t + W_{\mathrm{t0}} \tag{1}$$

where W_{t0} denotes the initial MMC energy. Based on this relationship, an integrator is constructed in the control layer to accumulate the deviation between the actual AC-side power P_{ac} and the reference DC-side power P_{dc}^*, expressed as $P_{\mathrm{h}}' = P_{\mathrm{dc}}^* - P_{\mathrm{ac}}$. The integrator output serves as the MMC energy reference W_{t}^*. Subsequently, a PI-based MMC energy control loop is established, where the energy error $e_{\mathrm{t}} = W_{\mathrm{t}} - W_{\mathrm{t}}^*$ drives the DC current control loop to regulate the DC current of the converter. As the DC current is explicitly controlled, the total stored energy within the MMC arms can be actively adjusted. Meanwhile, the physical dynamics inside the MMC occur synchronously. The DC current adjustment determines the DC power P_{dc}, and the power deviation between the AC and DC ports, $P_{\mathrm{h}} = P_{\mathrm{dc}} - P_{\mathrm{ac}}$, induces variations in the actual MMC energy W_{t}. The function of the energy control loop is therefore to continuously correct the DC power P_{dc} so that $e_{\mathrm{t}} \to 0$ (i.e., $W_{\mathrm{t}} \to W_{\mathrm{t}}^*$), which in turn ensures that P_{dc} converges to its reference value P_{dc}^*. When the energy control loop responds sufficiently fast, the DC-side power P_{dc} of the T/E/R-ICs will always track P_{dc}^*, effectively decoupling the DC power from AC-side power disturbances.

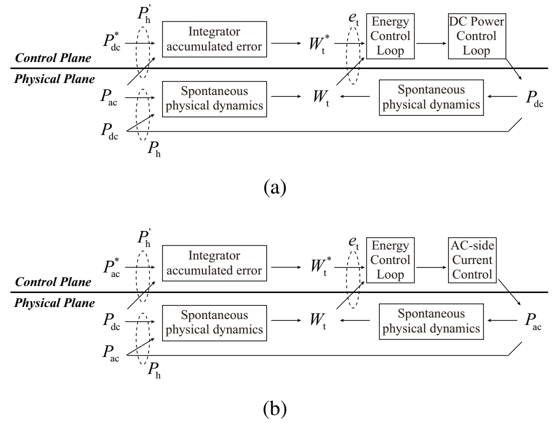

Fig. 2. Power buffering control strategy based on active MMC energy utilization. (a) Control scheme for T/E/R-ICs (Vf-P). (b) Control scheme for the G-IC (PQ-U_{dc}).

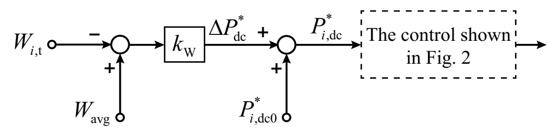

Fig. 3. Multi-IC energy coordination control scheme.

For the G-IC, since it regulates the DC-bus voltage within the TS (DC voltage control), its DC-side power is treated as an unknown variable that inherently includes the power fluctuations arising from other MMCs and DC-bus losses. In contrast, its AC-side power is expected to be precisely controlled to achieve a specified power exchange between the FTPSS and the upper-level grid. Fig. 2(b) illustrates the MMC energy-based buffering control method for the G-IC (PQ-U_{dc}). The principle is similar to that of the T/E/R-ICs, except that the deviation power is defined as $P_{\mathrm{h}}' = P_{\mathrm{dc}} - P_{\mathrm{ac}}^*$, which is computed from the actual DC power P_{dc} and the AC-side power reference P_{ac}^*. This deviation is integrated to generate the energy reference, which then drives an AC current control loop to regulate the AC power P_{ac}. When the energy control loop is fast enough, P_{ac} can be regarded as always equal to its reference P_{ac}^*.

Although each IC possesses power buffering capability under the control structure shown in Fig. 2, their stored energies may diverge under uncertain RES and TR power disturbances. To address this issue, a multi-IC energy coordination control scheme is developed, as depicted in Fig. 3. In this scheme, each T/E/R-IC adjusts its DC power reference according to the deviation between its own energy $W_{i,\mathrm{t}}$ and the system average

979-8-3315-8138-1

energy$W_{\mathrm{avg}} = \frac{1}{N}\sum_{i=1}^{N} W_{i,\mathrm{t}}$. A droop-based auxiliary control generates an additional DC power reference ΔP^*_{dc}, leading to the updated reference:

$$P^*_{i,\mathrm{dc}} = P^*_{i,\mathrm{dc0}} + \Delta P^*_{i,\mathrm{dc}} = P^*_{i,\mathrm{dc0}} + k_{\mathrm{W}}(W_{\mathrm{avg}} - W_{i,\mathrm{t}}) \quad (2)$$

where k_{W} denotes the energy coordination coefficient and $P^*_{i,\mathrm{dc0}}$ represents the nominal DC power setpoint. The physical interpretation of this control is that when the energy of one converter exceeds the average value, its DC power reference is adjusted to discharge additional power, thereby restoring its energy toward W_{avg}.

Compared with conventional approaches, G-IC and T/E/R-ICs enable accurate decoupling between AC and DC power as well as complete isolation of uncertain power disturbances. On this basis, the electrostatic energy stored in the arms of multiple MMCs within a traction substation can be equivalently aggregated into a larger energy buffer, which is exploited to absorb external power uncertainties, such as those arising from traction loads and renewable energy sources.

III. Traction-Station-Level Power Buffer Control under External Disturbances

A. Power Buffer Control Based on G-IC Operating Point Regulation

In Section II, we introduced power buffering control methods for T/E/R/G-ICs and a multi-IC energy coordination control approach to suppress external AC power disturbances and achieve coordinated energy operation among multiple ICs. However, the AC-side power reference of the G-IC, $P^*_{\mathrm{G,ac}}$, must be appropriately specified. The power balance equation at the TS terminals is given by:

$$P_{\mathrm{G,ac}} + \sum_{i\in\{\mathrm{T,E,R}\}} P_{i,\mathrm{ac}} + P_{\mathrm{m}} = 0 \quad (3)$$

where P_{m} represents the additional power provided by the MMC capacitors within the system to always satisfy the above equation. This term also accounts for the total system losses, including DC bus losses and individual IC losses. Based on the analysis in Section II, $P_{\mathrm{G,ac}}$ is approximately equal to its reference $P^*_{\mathrm{G,ac}}$. Clearly, $P^*_{\mathrm{G,ac}}$ must be carefully set, otherwise, an excessively large P_{m} will induce a continuous increase or decrease in the total IC energy, potentially causing IC operational failures. To address this, a TS-level buffering control method based on G-IC operating point regulation is proposed, as illustrated in Fig. 4. The method consists of a low-frequency power component control (LPCC) module and an energy balance control (EBC) module.

In the LPCC module, the AC-side powers of T-IC and R-IC, $P_{\mathrm{T,ac}}$ and $P_{\mathrm{R,ac}}$, are filtered through low-pass filters (LPFs) to remove high-frequency components. The resulting low-frequency main components, $P_{\mathrm{T,ac,L}}$ and $P_{\mathrm{R,ac,L}}$, are then used as the AC-side power control targets of the G-IC. The low-frequency AC power reference of the G-IC, $P^*_{\mathrm{G,ac,L}}$, can be expressed as:

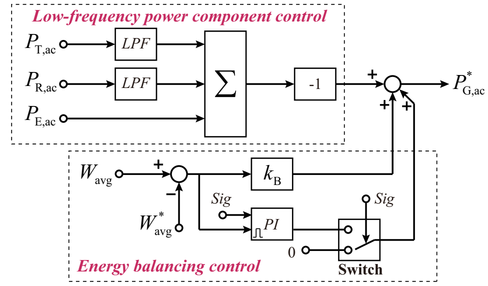

Fig. 4. G-IC-based TS power buffer control via AC-port operating point regulation.

$$P^*_{\mathrm{G,ac,L}} = -\left(\sum_{i\in\{\mathrm{T,R}\}} P_{i,\mathrm{ac,L}} + \sum_{i\in\{\mathrm{E}\}} P_{i,\mathrm{ac}}\right). \quad (4)$$

In Eq. (6), considering that the ESS power can be precisely controlled, only the port powers of the R-IC and T-IC corresponding to RES and TR require LPF processing. Under this method, high-frequency power components from external disturbances are absorbed by the equivalent energy buffer pools formed by the IC capacitors within the TS. This prevents the AC-side disturbance power from directly affecting the ESS or grid-side converters, avoiding high-frequency interference on their power setpoints and the need for rapid power adjustments. The low-frequency component obtained after first-order filtering is shown by the red curve. The transfer function of LPF is:

$$G(s) = \frac{1}{1+\tau s}. \quad (5)$$

B. Traction-Station-Level Energy Balance Control via EBC

Although the LPCC enables the G-IC to respond only to the low-frequency components of RES and TR power, significantly avoiding DC-side operating point adjustments of the G-IC and ESS caused by external power disturbances, the limited energy buffer capacity of MMC capacitors within the TS necessitates ensuring system energy stability during continuous operation. To this end, within the EBC module, an additional component generated by a droop controller, $\Delta P^*_{\mathrm{G,ac}}$, is added to the AC-side power reference of the G-IC:

$$\Delta P^*_{\mathrm{G,ac}} = k_{\mathrm{B}}\left(W_{\mathrm{avg}} - W^*_{\mathrm{avg}}\right) \quad (6)$$

where k_{B} denotes the EBC droop coefficient and W^*_{avg} is the reference value of the TS average energy. Physically, the EBC ensures that when the TS average energy W_{avg} deviates from its reference W^*_{avg}, the G-IC produces damping power to restore the system energy toward W^*_{avg}. A larger k_{B} increases the damping power and accelerates energy recovery. However, excessively large k_{B} reduces the TS's buffering capability for slowly varying external disturbances. This is because the EBC forces W_{avg} to quickly return to W^*_{avg}, causing disturbance power from the R-IC or T-IC to be reflected

979-8-3315-8138-1

TABLE I
SIMULATION PARAMETERS

Parameter	Value	Parameter	Value
DC nominal voltage u_{dc}	80 kV	Energy upper limit $W_{\mathrm{avg,max}}$	1.3
AC nominal voltage u_{ac}	25 kV	Energy lower limit $W_{\mathrm{avg,min}}$	0.7
Number of submodules N_{sm}	80	Arm inductance L_{a}	5.9 mH
Submodule capacitance C_{sm}	25 mF	Output inductance L_{s}	11.9 mH
Nominal frequency f_0	50 Hz	Arm resistance R_{a}	0.5 Ω
Nominal capacity S_0	50 MVA	Output resistance R_{s}	0.03 Ω

onto the G-IC with little buffering, thereby compromising the TS's power buffering function. Conversely, if k_{B} is too small, insufficient damping may result in large deviations of W_{avg} under continuous external disturbances, potentially exceeding the maximum allowable energy regulation margin. To address this, an additional PI controller is incorporated to implement saturation limiting. As illustrated in Fig. 4, when W_{avg} reaches the upper or lower limits of the energy regulation margin, $W_{\mathrm{avg,max}}$ or $W_{\mathrm{avg,min}}$, the control signal Sig is set to 1. This clears the integrator's current state and switches the input from zero to the PI controller input. The PI controller then accumulates the power reference $\Delta P^*_{\mathrm{G,ac,PI}}$ to rapidly drive W_{avg} back toward W^*_{avg}. Once recovery is complete, Sig is reset to zero, awaiting the next energy-limit event. Therefore, combining the outputs of the LPCC and EBC components, the AC-side power reference of the G-IC can be expressed as:

$$P^*_{\mathrm{G,ac}} = P^*_{\mathrm{G,ac,L}} + \Delta P^*_{\mathrm{G,ac}} + s(t) \cdot \Delta P^*_{\mathrm{G,ac,PI}} \tag{7}$$

where $s(t) \in \{0, 1\}$ represents the logical value of the Sig signal.

IV. SIMULATION VERIFICATION

To validate the effectiveness of the proposed method, a four-IC system comprising T-, E-, R-, and G-ICs was established on the MATLAB/Simulink platform. The simulation parameters are summarized in Table 1.

A. Validation under High-Frequency Disturbances

Fig. 5 illustrates the simulation results under continuous low-amplitude external power disturbances. At $t = 2$ s, the R-IC generates three consecutive power disturbances, each with a duration of 0.05 s and an amplitude of 0.1 p.u., to emulate potential operational fluctuations of the RES. At $t = 3$ s, the disturbance duration is reduced to 0.025 s. Fig. 5(a) presents the AC-side power of the R-IC, $P_{\mathrm{R,ac}}$, along with the low-frequency component extracted by the LPF (red curve). It can be observed that the original external power disturbances, which exhibit high power change rates (nearly step-like), are filtered to extract the dominant low-frequency components. This effectively prevents significant adjustments of the G-IC operating point. As shown in Fig. 5(b), the AC-side power of the G-IC, $P_{\mathrm{G,ac}}$, undergoes only minor adjustments in response to the low-frequency components, with a maximum power increment of merely 0.05 p.u., which is significantly

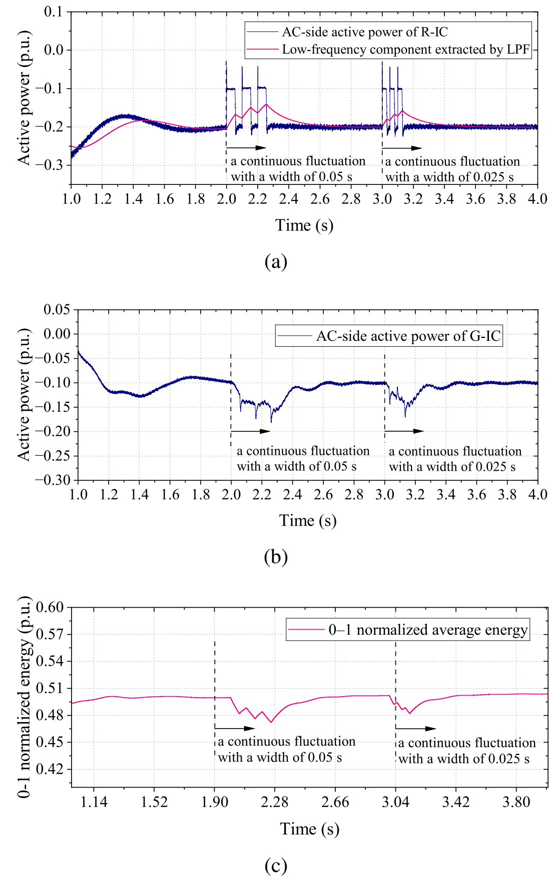

Fig. 5. Simulation results of the 4-IC system under small-amplitude, high-frequency external disturbances. (a) Power curve of the R-IC. (b) Power curve of the G-IC. (c) Normalized system average energy (0–1 scale).

smaller than the 0.1 p.u. increment induced by the original R-IC disturbance. Fig. 5(c) shows the system average energy, W_{avg}, indicating that the MMC capacitors within the TS effectively buffer the power deviations to maintain overall system power balance. In contrast, under the conventional approach without power buffering, rapidly varying external power disturbances would cause pronounced fluctuations in the AC power operating point of the G-IC.q

B. Validation under Large-Amplitude Disturbances

Fig. 6 presents the simulation results of the four-IC system under large-amplitude external power disturbances. At $t = 2$ s, the AC-side power of the T-IC, $P_{\mathrm{T,ac}}$, is increased stepwise from 0.2 p.u. to 0.7 p.u. to emulate a sudden, large load increase during TR start-up. Subsequently, at $t = 2.5$ s, $P_{\mathrm{T,ac}}$ is restored to 0.2 p.u. to simulate a rapid load decrease. The LPF time constant is set to $\tau = 0.125$ s. It can be observed that, for both load step-up and step-down scenarios, the LPF effectively reduces the rate of power change (green curve in Fig. 6(a)). Consequently, the G-IC only needs to respond slowly to the low-frequency power components, while the deviation power (the difference between the red and green curves) is absorbed by the MMC capacitors of all ICs within the TS. The AC-side power of the G-IC, $P_{\mathrm{G,ac}}$, demonstrates the effectiveness of the

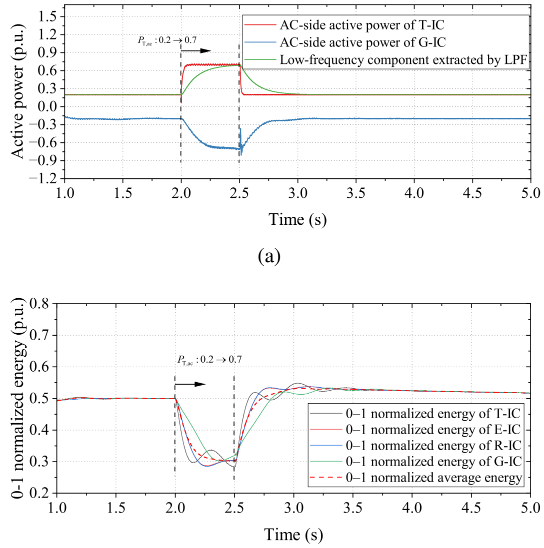

(b)

Fig. 6. Simulation results of the 4-IC system under large external power disturbances. (a) System power curves. (b) System energy curves.

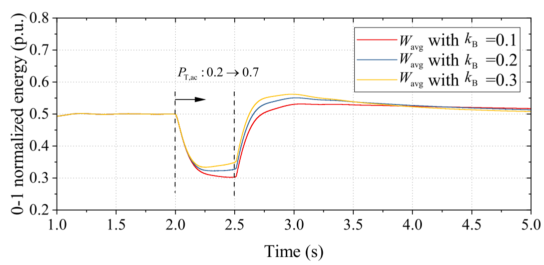

Fig. 7. System average energy trajectories under different k_B settings.

proposed method, as its rate of change is significantly reduced. Fig. 6(b) shows the energies of all ICs and the system average energy, normalized between 0 and 1 based on the maximum and minimum energy regulation limits. Between $t = 0.2$ s and 0.25 s, the energies of all ICs decrease continuously to supply the sudden 0.5 p.u. increase of $P_{T,ac}$. Meanwhile, the EBC is actively restoring the average energy, W_{avg}, toward the reference value, W^*_{avg}. In this simulation, the EBC droop coefficient is set to $k_B = 0.1$. Over time, W_{avg} gradually converges toward the reference value of 0.5 p.u.

Fig. 7 illustrates W_{avg} curves under different k_B settings. It is observed that larger values of k_B provide greater damping power, accelerating system energy recovery. When $k_B = 0.3$ (yellow curve), the minimum value of W_{avg} is significantly increased, and after $t = 2.5$ s, it achieves the fastest convergence speed.

V. Conclusion

To address the continuous operating point disturbances experienced by the grid converters and energy storage systems within a traction substation due to power fluctuations from renewable energy sources and electric trains, a traction-station-level power buffering control method based on multi-MMC coordination for FTPSS is proposed. The method is developed on the basis of energy-coordinated control frameworks for both T/E/R-ICs and the G-IC. Simulation results demonstrate that, with the proposed method, the grid-side ports of the TS respond only to the dominant low-frequency components of RES and traction loads, while the remaining deviation power is collectively absorbed by the MMC capacitors within the system. Furthermore, the method endows the TS with damping power: under continuous external power disturbances, the energy balance control component ensures that the system average energy is consistently restored to the reference value. Additionally, larger damping coefficients accelerate the system's energy recovery. These results verify the effectiveness of the proposed method in enhancing the FTPSS's adaptability to uncertainties associated with RES and electric locomotive operations. Future work will further validate the proposed method through prototype experiments, and the corresponding results will be summarized and reported in subsequent publications.

References

[1] Y. Liu, M. Chen, Z. Cheng, Y. Chen, and Q. Li, "Robust energy management of high-speed railway co-phase traction substation with uncertain PV generation and traction load," *IEEE Trans. Intell. Transp. Syst.*, vol. 23, no. 6, pp. 5079–5091, Jun. 2022.

[2] J. Li, Y. Wei, X. Li, C. Lu, X. Guo, Y. Lin, and M. Molinas, "Modeling and stability prediction for the static-power-converters interfaced flexible AC traction power supply system with power sharing scheme," *Int. J. Electr. Power Energy Syst.*, vol. 154, p. 109401, Dec. 2023.

[3] M. Chen, Z. Liang, Z. Cheng, J. Zhao, and Z. Tian, "Optimal scheduling of FTPSS with PV and HESS considering the online degradation of battery capacity," *IEEE Trans. Transport. Electrific.*, vol. 8, no. 1, pp. 936–947, Mar. 2022.

[4] M. Chen, Z. Cheng, Y. Liu, Y. Cheng, and Z. Tian, "Multitime-scale optimal dispatch of railway FTPSS based on model predictive control," *IEEE Trans. Transport. Electrific.*, vol. 6, no. 2, pp. 808–820, Jun. 2020.

[5] R. Li, Q. Sun, Q. Chen, and M. Xia, "A Methodology for Power Dispatch Based on Traction Station Clusters in Flexible Traction Power Supply System," *IEEE Transactions on Transportation Electrification*, pp. 1–1, 2025.

[6] J. Lai, M. Chen, X. Dai, L. Liu, and N. Zhao, "Power flow optimization and control strategy for energy router in dual mode traction power supply system," *IEEE Trans. Intell. Transport. Syst.*, vol. 24, no. 11, pp. 12 284–12 293, Nov. 2023.

[7] P. Guo, Z. Tian, Z. Yuan, X.-Y. Zhang, and D. Sharifi, "Research on Symmetric Bipolar MMC-M2Tdc-Based Flexible Railway Traction Power Supply System," *IEEE Transactions on Transportation Electrification*, vol. 10, no. 1, pp. 1043–1055, Mar. 2024.

[8] H. Zhang, W. Xiang, and J. Wen, "Dual Grid-Forming Control With Energy Regulation Capability of MMC-HVDC System Integrating Offshore Wind Farms and Weak Grids," *IEEE Trans. Power Syst.*, vol. 39, no. 1, pp. 261–272, Jan. 2024.

[9] H. Zhang, W. Xiang, Y. Wang, and J. Wen, "Energy-Utilizing Frequency Support for MMC-MTDC System Integrating Asynchronous Grids," *IEEE Trans. Energy Convers.*, vol. 39, no. 4, pp. 2591–2604, Dec. 2024.

[10] M. M. Kabsha and Z. H. Rather, "A New Control Scheme for Fast Frequency Support From HVDC Connected Offshore Wind Farm in Low-Inertia System," *IEEE Transactions on Sustainable Energy*, vol. 11, no. 3, pp. 1829–1837, Jul. 2020.

[11] E. Sanchez-Sanchez, E. Prieto-Araujo, and O. Gomis-Bellmunt, "The Role of the Internal Energy in MMCs Operating in Grid-Forming Mode," *IEEE Journal of Emerging and Selected Topics in Power Electronics*, vol. 8, no. 2, pp. 949–962, Jun. 2020.

[12] R. Yang, G. Shi, C. Zhang, G. Li, and X. Cai, "Internal Energy Based Grid-Forming Control for MMC-HVDC Systems With Wind Farm Integration," *IEEE Trans. on Ind. Applicat.*, vol. 59, no. 1, pp. 503–512, Jan. 2023.